THE JOURNAL OF PHYSICAL CHEMISTRY B

pubs.acs.org/JPCB Article

Direct Simulations of Phase Behavior of Mixtures of Oppositely Charged Proteins/Nanoparticles and Polyelectrolytes

Published as part of The Journal of Physical Chemistry virtual special issue "Carol K. Hall Festschrift".

Rituparna Samanta and Venkat Ganesan*

Cite This: *J. Phys. Chem. B* 2020, 124, 10943−10951 Read Online

ACCESS | Metrics & More | Article Recommendations | Supporting Information

ABSTRACT: We use direct simulations of particle−polyelectrolyte mixtures using the single chain in mean field framework to extract the phase diagram for such systems. At high charges of the particles and low concentration of polymers, we observe the formation of a coacervate phase involving the particles and polyelectrolytes. At low particle charges and/or high concentration of polymers, the mixture undergoes a segregative phase separation into particle-rich and polymer-rich phases, respectively. We also present results for the influence of particle charge heterogeneity on the phase diagram.

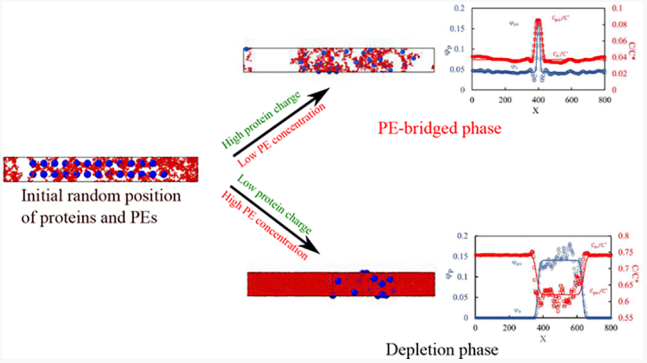

1. INTRODUCTION

Mixtures of globular proteins and polyelectrolytes (PEs) are widely used in food products to modulate properties such as consistency, taste, and so on. For instance, the structures resulting from the complexation of casein protein and pectin(ate) polysaccharides are used to control the texture and stability of dairy products.[1−4] Moreover, the in-mouth perception and flavor release characteristics in food materials have been shown to depend on the rheology of the protein−PE complexes.[1,5] In other contexts, immobilization of proteins using oppositely charged polyelectrolytes is used as a strategy for the stabilization of enzymes in biosensors,[6] selective purification of proteins, drug delivery, and so on.[7−9]

Design of the above applications requires knowledge of the equilibrium phase behavior of mixtures of proteins and PEs. In general, when the interactions between the proteins and polyelectrolytes are favorable, due to either electrostatic or enthalpic driving forces, the system separates into two phases: one which is enriched in both proteins and PEs, and called the "coacervate", and the other phase which is dilute in proteins and PEs. In contrast, when the interactions between the protein and PEs are unfavorable, they separate into two phases enriched respectively in proteins and PEs (termed as segregative phase separation).

In view of the practical implications, there have been a significant number of experimental studies aimed at understanding the phase behavior of protein−polyelectrolyte mixtures.[10,11] Such studies have demonstrated that the interactions and the resulting phase behavior of protein−polyelectrolyte mixtures can be influenced by a variety of factors such as the charge of the individual entities, solution conditions, geometry of the globular proteins, and temperature.[4,10,11] Despite these insightful studies, outstanding issues still remain regarding the influence of parameters such as the solution pH, protein−PE mixing ratio, protein charge heterogeneity, and the charge of the PE in influencing the phase behavior in such systems.[4,12−14]

Because the accompanying parameter space of protein−PE mixtures is extremely vast, there have also been a few simulation studies that have probed the influence of different protein and polyelectrolyte characteristics on the resulting phase behavior.[15−19] Full scale simulations involving realistic (or even coarse-grained) representations of proteins, polyelectrolytes, counterions, and salt are computationally intractable. Some studies have circumvented such challenges by approximating the interactions between the proteins by the effective, polymer-mediated two-body potentials deduced at the dilute limit and using such interactions in simulations of just the proteins.[16,20,21] However, such approximations ignore the influence of electrostatic screening and crowding effects arising from the presence of multiple particles.

Received: September 11, 2020
Revised: November 2, 2020
Published: November 18, 2020

https://dx.doi.org/10.1021/acs.jpcb.0c08317
J. Phys. Chem. B 2020, 124, 10943−10951

Motivated by the above issues, our group developed a single chain in mean-field (SCMF)-based *multiparticle* simulation framework which accounts explicitly for the presence of multiple (proteins) particles, polymers, and counterions.[18,22,23] In previous publications from our group,[18,22] we studied the effect of different independent variables such as the net charge of the particles and concentration of the polymers on the phase behavior of protein−polyelectrolyte complexes. The characterization of the phase behavior was presented in terms of radial distribution functions (RDF), cluster size distributions, and the PE bridging characteristics. On the basis of such *indirect* measures, our studies concluded that at low concentrations of the polymer and high net charge of the protein protein−PE mixtures are likely to form a coacervate-like phase in which the proteins are bridged by the PEs. In contrast, at low protein charges and high polymer concentrations, the polymer-induced depletion interactions dominate, and the mixture undergoes segregative phase separation to form protein aggregates. In more recent studies,[23,24] we extended the above framework to study the influence of protein charge heterogeneity and charge regulation phenomena arising from the dissociability of charge groups on proteins and PEs. Our results in such contexts demonstrated that amphoteric proteins with both positive and negative charge patches exhibited increased affinity to form polymer-bridged phases relative to homogeneously charged proteins.

Despite the understanding arising from the above-mentioned studies, it is still unresolved whether the morphological measures probed within a single phase system (or at the level of two particles at infinite dilution) suffice to capture the true phase coexistence characteristics in such systems.[18,23,24] Calculating true phase diagrams based on particle-based simulations, however, often involves the calculation of free energies or other alternative methods to ensure the equality of chemical potentials among the coexisting phases.[16,21,25] While significant progress has been achieved,[26−29] particle-based simulations are still computationally expensive, especially for complex systems such as protein−polymer and nanoparticle−polymer mixtures which involve interactions at many different length scales.

Recently, Koski and Riggleman et al. presented a field-based framework which probed the phase diagram for polymer grafted nanoparticle in a polymer matrix.[30] Their simulations implemented a hybrid particle-field method called theoretically informed Langevin dynamics (TILD).[31,32] To calculate the phase diagram, a cuboidal simulation box was used and initialized with the particle-rich phase in the center of the box, surrounded by a polymer-rich phase. The particles and the polymers were then allowed to equilibrate, and the phase diagram was extracted based on the coexisting volume fractions in the resulting configurations with an explicit interface.

Inspired by the above work of Riggleman and co-workers,[30] in this work, we explored whether similar direct simulations of phase separation in protein−PE mixtures can be used as a tool to extract phase behavioral information to complement (and confirm) the conclusions derived from morphological characteristics presented in our previous articles. Toward this objective, we adapted the methodology presented by Koski et al.[30] and embedded it within the self-consistent mean-field simulation approach presented in our previous publications.[18,22−24] Using such a framework, we study the influence of the net charge and charge heterogeneity on the protein on the phase behavior of protein−PE complexes. Admittedly, an accurate determination of phase diagram requires consideration of finite size effects arising from the box dimensions. However, in this study, we do not undertake such a task and instead use the simulation framework primarily as a means to validate, compare, and complement the findings of the structural features presented in our previous articles.

The rest of the article is organized as follows. In section 2, we briefly discuss the model details, and the parameters used for the numerical methodologies are shown in section 3. In section 4, we begin by presenting the results for phase separation of mixtures of PEs and homogeneously charged proteins. In section 4.2 we present results for the influence of surface charge heterogeneity of proteins. We conclude with a summary of our findings in section 5.

2. MODEL DESCRIPTION

2.1. Model Details for Protein−PE Mixtures. Similar to our earlier studies,[18,23,24] we focus on mixtures of globular proteins and PEs and adopt a simple model of (charged) spherical nanoparticles to model such entities. Hereafter, because of this simplistic model representation, we refer to the proteins as particles. To study the influence of protein charge heterogeneity on the phase behavior, we use the "toy" model described in our previous publications.[23] Explicitly, the charge heterogeneity on proteins is represented as charge patches distributed on the surface of the sphere over an angle α (shown in Figure 1). We use "patches" to denote the region over which

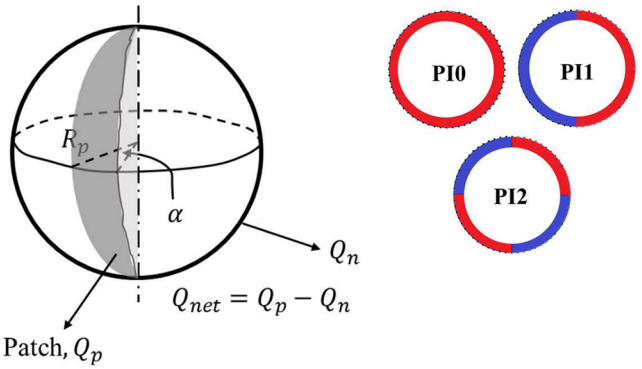

Figure 1. Model of patchy particles. The red color shows patches of positive charge, and the blue color depicts negative or neutral patches.

positive (or negative) charges are distributed. The net positive charge (distributed uniformly over all patches) is denoted as Q_p. The rest of the particle surface has a negative charge Q_n. The net charge of the particle is denoted as $Q_{net} = Q_p - Q_n$. The nomenclature "PI*N*" is used to refer to the geometric variants that contain "*N*" patches of negative charges. As an example, "PI0" represents a homogeneously charged positive particle, "PI1" are particles with one positive and one negative patch, and "PI2" represents particles with two positive and two negative patches.

For our simulations, we consider a canonical ensemble of N_p charged spherical particles of radius R_p and n negatively charged polymer chains of m monomers each and radius of gyration R_g in a simulation box with periodic boundary conditions on all sides. To maintain electroneutrality of the system, n_p and n_m point counterions for the particles and polymers are included. In this work, we did not consider the influence of additional salt. Hereafter, the concentration of the polymer is presented in units of the overlap concentration C^*

https://dx.doi.org/10.1021/acs.jpcb.0c08317
J. Phys. Chem. B 2020, 124, 10943−10951

of an ideal linear polymer chain solution. The charge on the monomers of the polymer is denoted as z_m. The volume fraction of the particles is denoted as ϕ_p. We assume the dielectric constant of the particle to be the same as that of the solvent.

We assume a flexible bead−spring chain model for the polyelectrolytes, in which the intramolecular interactions in the polymer chains are modeled through a bead−spring model, with bonded Hookean interactions:

$$\frac{H_b}{k_BT} = \frac{3}{2b^2}\sum_{i=1}^{n}\sum_{s=1}^{m-1}[\mathbf{r}_i(s) - \mathbf{r}_i(s+1)]^2 \tag{1}$$

where $\mathbf{r}_i(s)$ represents the coordinate of the s^{th} bead on the i^{th} polymer. Excluded volume interactions between the polymer segments are incorporated through a simplistic implicit solvent interaction potential of the form

$$\frac{\bar{u}(\mathbf{r})}{k_BT} = u_0\delta(\mathbf{r}) \tag{2}$$

where u_0 is commonly known as the excluded volume parameter.[33] In the above framework, the nonbonded interactions between the polymer segments can be formally recast as

$$\frac{H_s}{k_BT} = \frac{u_0}{2}\int \hat{\rho}_{poly}{}^2(\mathbf{r})\,d\mathbf{r} \tag{3}$$

where $\hat{\rho}_{poly}$ is the microscopic polymer segment density[34]

$$\hat{\rho}_{poly}(\mathbf{r}) = \sum_{i=1}^{n}\sum_{s=1}^{m}\delta[\mathbf{r} - \mathbf{r}_i(s)] \tag{4}$$

The instantaneous density of particles is similarly quantified through a particle volume fraction field as

$$\rho_{part}(\mathbf{r}) = \sum_{i=1}^{N_p}\int_{r_i}^{r_i+R_p}\hat{\rho}_{part}(\mathbf{r})h(|\mathbf{r}' - \mathbf{r}_i|)\,d\mathbf{r}' \tag{5}$$

where $\hat{\rho}_{part}(\mathbf{r}) = \delta(\mathbf{r} - \mathbf{r}_i)$ and $h(r) = 1$ when $|r| < R_p$. The counterions were considered to be as point charges, and their microscopic densities are given by

$$\rho_{mi}(\mathbf{r}) = \sum_{i=1}^{n_m}\delta(\mathbf{r} - \mathbf{r}_i)$$

$$\rho_{pi}(\mathbf{r}) = \sum_{i=1}^{n_p}\delta(\mathbf{r} - \mathbf{r}_i) \tag{6}$$

For modeling the particle−counterion and particle−monomer interactions, the particles are envisioned as spherical objects with a thin layer of penetrable soft core surrounding an impenetrable hard core. The repulsive interactions between the particle and the polymer monomers and counterions are modeled through a potential of the form

$$W_{cp}(\mathbf{r}) = 50\left[1 - \tanh\left(2\frac{\mathbf{r} - \alpha R_p}{\beta}\right)\right]k_BT \tag{7}$$

The coefficients α and β control the steepness and range over which the repulsive potential decays from 100 k_BT to 0 k_BT. We have used $\alpha = 0.9$ and $\beta = 0.5$ for the simulation, which ensures that the particle cores are almost impenetrable to counterions and polymers. In addition, the direct interparticle interactions are modeled through a hard-sphere interaction:

$$\frac{H_{pp}}{k_BT} = \frac{1}{2}\sum_{i=1}^{N_p}\sum_{j=1(j\neq i)}^{N_p}U_{HS}(|\mathbf{r}_i - \mathbf{r}_j|) \tag{8}$$

where

$$U_{HS}(r) = \begin{cases} 0, & \text{if } r \geq 2R_p \\ \infty, & \text{if } r < 2R_p \end{cases} \tag{9}$$

For the simulations of protein−polyelectrolyte mixtures, we have used the single chain in mean field (SCMF) approach introduced by Mueller and co-workers.[18,22,35−37] In the SCMF framework, the nonbonded pairwise interactions are replaced with fluctuating potential fields which are conjugate to the corresponding density fields.[35] The electrostatic energy arising from the charges is represented in terms of the conjugate electrostatic potential field $\varphi(\mathbf{r})$ and the associated energy:

$$\frac{H_{el}}{k_BT} = \int d\mathbf{r}\left[\rho_e(\mathbf{r})\varphi(\mathbf{r}) - \frac{1}{8\pi l_b}|\nabla\varphi(\mathbf{r})|^2\right] \tag{10}$$

where $\rho_e(\mathbf{r})$ is the total charge density arising from particles, polymers, and counterions (in units of e) and is given as

$$\rho_e(\mathbf{r}) = z_{part}(\mathbf{r})\rho_{part}(\mathbf{r}) \pm \sum_{ion} z_{ion}\rho_{ion}(\mathbf{r}) - z_m\hat{\rho}_{poly}(\mathbf{r}) \tag{11}$$

where z_{ion} is the valency of each ion (co- or counterions) and $z_{part}(\mathbf{r})$ is the local fractional charge of the particle, which in turn depends on the sign and magnitude of the particle patch at $\mathbf{r}$. The field $\rho_{ion}(\mathbf{r})$ denotes the local density of co- and counterions. The electrostatic potential $\varphi(\mathbf{r})$, in units of k_BT/e, is obtained as the solution of Poisson's equation:

$$\nabla^2\varphi(\mathbf{r}) = -4\pi l_b\rho_e(\mathbf{r}) \tag{12}$$

In eq 12, l_b is the Bjerrum length, defined as $e^2/4\pi\varepsilon_0\varepsilon_r k_BT$, where ε_r is the relative dielectric constant of the medium and ε_0 is the vacuum permittivity. For water, at 300 K, $l_b \approx 0.7$ nm. To embed our model for particle charge heterogeneity within a grid-like representation of the SCMF approach, we divided the surface of each sphere into grids and distributed the charges such that all the grid points covering the positive charge patch has a fractional charge totaling to Q_p and the grid points covering the negative charge patch have a fractional charge totaling to Q_n.

2.2. Simulations of Phase Coexistence. In this work, we characterized the phase behavior of the protein polymer system using the methodology proposed in Koski et al.[30] For all the phase calculations, we fixed the volume fraction of particles in the simulation box $\varphi_p = 0.05$.

We begin the simulation by placing the particles in a cubic lattice configuration at the center of the box and polymers and the counterions randomly in the rest of the space. We have also repeated the simulations with other initial conditions (counterions are placed randomly in the box for all cases): (a) where the polymers are placed in the center of the box along with the particles and (b) where the polymers are placed randomly in the box. For all the initial conditions, we obtained a similar concentration profile of the protein and polymers (as seen in Figure S1), which indicates that our results are independent of the initial conditions. Subsequently, we allow the system to

https://dx.doi.org/10.1021/acs.jpcb.0c08317
J. Phys. Chem. B 2020, 124, 10943−10951

equilibrate for a fixed number of iterations, the details of which are provided in section 3. During the production run, the ensemble average of the in plane variations of concentration of particles, polymers and other species (such as positive and negative counterions) are calculated. The ensemble average is effected by adjusting the $y-z$ average concentration profiles such that the peak of the volume fraction of particles is shifted to the center of the simulation box, i.e., at $x = L_x/2$. In this manner, the drift of the system, if any, is eliminated in the calibration of the compositions at coexistence. The system is assumed to have equilibrated when the ensemble average of the concentration profile almost remain constant. (The maximum difference in an average concentration of particles at the center of the box is ≈0.9−1.0% among consecutive steps.) The difference in the average of other properties such as the radius of gyration R_g of the PEs is $<1 \times 10^{-2}$. To obtain the values of the coexisting concentrations of particles and polymers, we fit the resulting concentration profiles to a function of the form[30]

$$\varphi(x) = \varphi_b + \frac{\varphi_{pa} - \varphi_b}{2}\left[\mathrm{erf}\left\{\frac{x - \frac{L_x}{2} + x_0}{\Delta}\right\} - \mathrm{erf}\left\{\frac{x - \frac{L_x}{2} - x_0}{\Delta}\right\}\right] \tag{13}$$

$$C_{pol}(x) = C_b + \frac{C_{pa} - C_b}{2}\left[\mathrm{erf}\left\{\frac{x - \frac{L_x}{2} + x_{pol0}}{\Delta_{pol}}\right\} - \mathrm{erf}\left\{\frac{x - \frac{L_x}{2} - x_{pol0}}{\Delta_{pol}}\right\}\right] \tag{14}$$

where φ_i (i = 'pa' or 'b') corresponds to the coexisting particle volume fractions, $L_x/2 \pm x_0$ is position of the interface, and Δ is a measure of the interfacial width. Similarly, C_i (i = 'pa' or 'b') corresponds to the normalized (by C^*) coexisting concentrations of the polymers in the two phases and $L_x/2 \pm x_{pol0}$. As an illustration, the solid lines in Figure 2 are a fit to the concentration and volume fraction profiles. Fits are obtained by using the generalized reduced gradient (GRG) nonlinear solver to minimize the sum of square of the residuals.

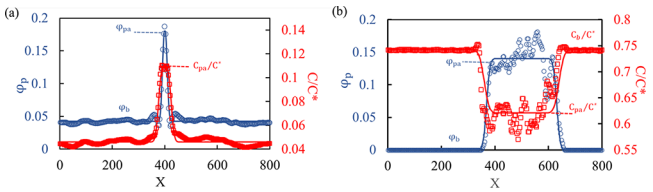

Figure 2. Ensemble average of the volume fraction of proteins and concentration of polymer averaged over the $y-z$ plane. The ensemble average is done by adjusting the peak of the volume fraction to $x = L_x/2$. The average properties are for PI0 particles with $Q_{net} = 60$ and bulk concentration of polymer set at (a) $C/C^* = 0.05$ and (b) $C/C^* = 0.70$. The particle volume fraction is presented by the blue markers and corresponds to the value on the left y-axis; the polymer concentration is presented by the red markers and corresponds to the value on the right y-axis. The solid lines for all cases are the best fit to the error functions.

In addition to the above characterization of the coexisting compositions, we probe the structure of particle−PE complexes by using the PE bridging fraction, B_r, defined as the fraction of PEs that can bind with more than one particle. We have used B_r in our previous publications as a proxy measure for the propensity for complexation.[22,23]

3. NUMERICAL METHODS AND PARAMETERS

The model described in the previous section is used in a Monte Carlo simulation approach in which the configuration space is sampled by using the Metropolis algorithm.[38] In the initial portion of the simulation, 10^4 Monte Carlo (MC) moves are effected such that only the polymers are moved while keeping the particles fixed in space. This pre-equilibration is done to ensure the removal of any particle−polymer overlaps. Subsequently, each Monte Carlo step (MCS) involves a MC move for all particles, a slithering snake move for all polymer chains, and 100 MC moves for all polymers and counterions. Every MC move of the particle includes a translation and rotation move (only for inhomogeneously charged particles) for all particles. Using such a sequence of moves, the system is equilibrated for 6×10^4 MCS. Subsequently, the properties are averaged over 7×10^4 MCS, constituting the production cycle. Using the position of the monomers, particles, and ions, the density fields, charge density fields, and electrostatic fields are updated after every move of the polymer and particles.

We use an anisotropic 3D Fourier transformation using the numerical 3D ($256 \times 32 \times 32$) fast Fourier transform (FFT) numerical method to solve Poisson's equation (eq 12).[18,22,39−41] For our study, we have used the Bjerrum length (l_b) as 0.7 nm, corresponding to that of water at 300 K. In this study, we have kept the value of $u_0 = 10$, representing a good solvent. We note that previous studies from our group suggested that excluded volume interactions exert only a small influence on the results.[18,22] The particles used in the simulation are of radii $R_p = 15$ nm and the homopolymers of $R_g = 24$ nm. The number of monomers in a polymer chain is set at $m = 60$ and the net charge of the polymer as $Q_{pol} = 60$. For the simulation, we have used a periodic cuboidal box of dimensions $L_x(800\text{ nm}) \times L_y(100\text{ nm}) \times L_z(100\text{ nm})$ with $L_x \approx 53 \times R_p$ divided into a $256 \times 32 \times 32$ grids. In this study, we did not probe the effect of varying R_p or R_g.

4. RESULTS AND DISCUSSION

4.1. Influence of Net Protein Charge Q_{net}. In this section, we present results for the effect of Q_{net} on the phase behavior of mixtures of *homogeneously* charged particles and oppositely charged polyelectrolytes. Our earlier study considered such systems,[18] and by characterizing the structures resulting in single phase simulations, we presented evidence for the formation of PE-bridged clusters form at high net charges and low bulk PE concentrations. Such phases were envisioned to correspond to the complex coacervate phase observed in experiments. In contrast, at higher polymer bulk concentrations and/or lower particle charges, the depletion interaction effects associated with exclusion of polymers from the particle cores became dominant. In such regimes, the particles formed "agglomerates" suggestive of segregative phase separation. For better visualization, we have added snapshots of the PE-bridged phase and segregative phase separation in Figure S2.

https://dx.doi.org/10.1021/acs.jpcb.0c08317
J. Phys. Chem. B 2020, 124, 10943−10951

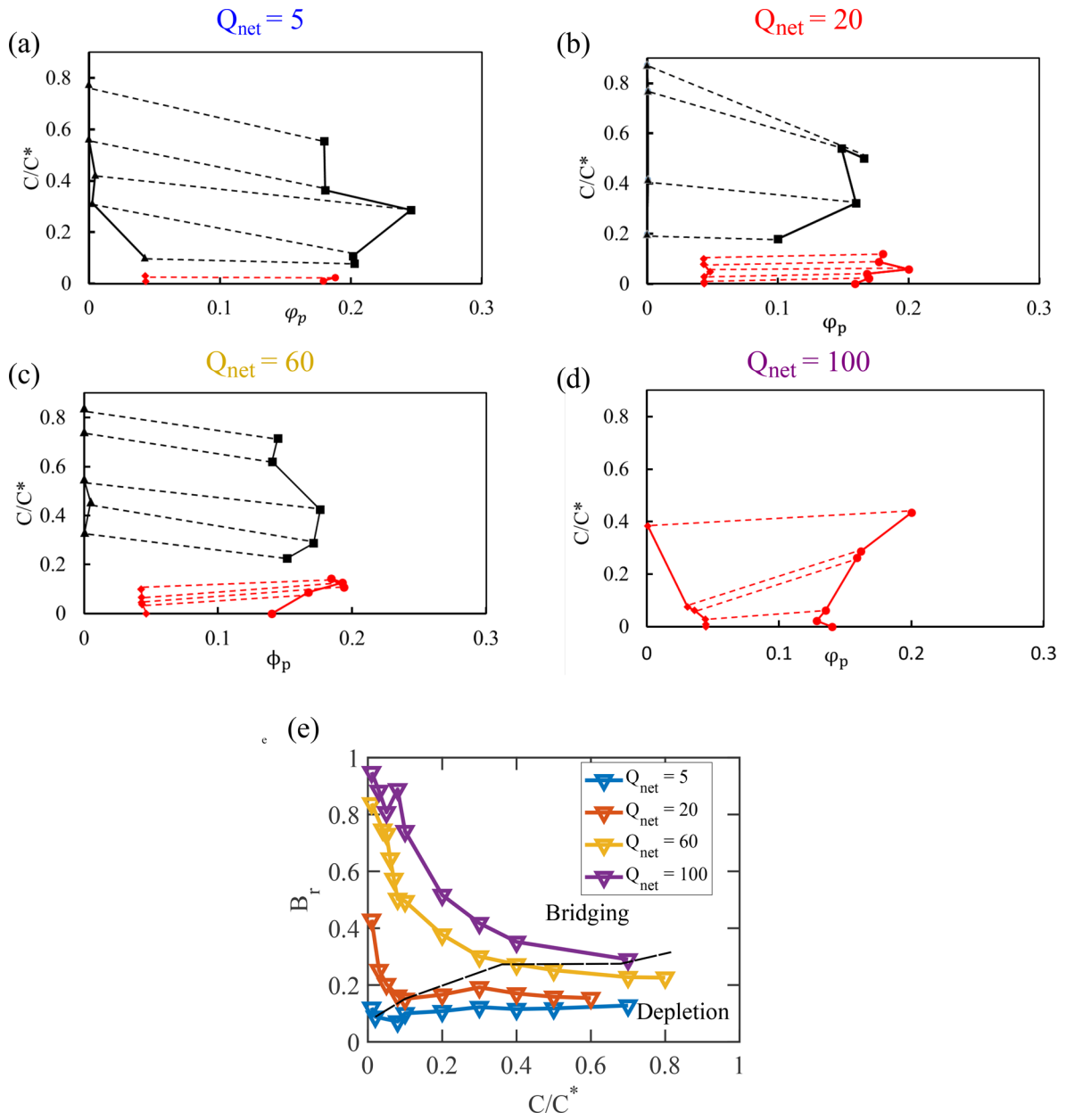

Figure 3. Phase diagram for PI0 particles with particle net charge (a) Q_{net} = 5, (b) Q_{net} = 20, (c) Q_{net} = 60, and (d) Q_{net} = 100. (e) Bridging fraction as a function of polymer bulk concentration for different values of net charge of PI0. The concentration range covers both the coacervate and segregative phase separation. The black long dashed line in (e) is used to distinguish between the coacervate and segregative phases.

Figure 3a displays the results from this study for the phase diagram for Q_{net} = 5 in the ϕ_p and C/C^* plane. As seen in the phase diagram, for polymer concentrations $C/C^* > 0.01$, the system undergoes a segregative phase separation to phases respectively rich in particles and polymers (as seen by the negative slope of the tie line in Figure 3a). Such phase behavior is also seen explicitly in the volume fraction profiles of the particles and polymer displayed in Figure S3b. However, at low polymer concentrations ($C/C^* < 0.01$), where the depletion interactions arising from the polymers is expected to be weaker, the concentration profiles presented in Figure S3a display a different behavior in which the concentration of polymer and the particle volume fractions are enhanced in the same region of the simulation box, indicating the formation of coacervate phases. Such characteristics are again seen to be reflected in the (positive) slope of tie lines.

The above phase behavioral features are also seen to be reflected in the polymer bridging fractions displayed in Figure 3e as a function of the concentration of polymers. Explicitly, for Q_{net} = 5, at a low concentration of polymers, the bridging fraction is seen to be relatively high—consistent with the formation of coacervates arising from polymer bridging. With increase in polymer concentration, the polymer bridging fractions are seen to decrease, and eventually the bridging fraction is seen to become insensitive to an increase in the concentration of polymers (shown by the region on the left of the black dashed line in Figure 3e). Such observations can be rationalized by noting that in the polymer-bridged coacervate phase (at low concentration of polymer), polymers are adsorbed to neutralize the charge of the particles. Hence, with an increase in the concentration of the polymers, the fraction of polymers forming a bridge between particles

https://dx.doi.org/10.1021/acs.jpcb.0c08317
J. Phys. Chem. B 2020, 124, 10943−10951

decreases due to an increase in the net concentration of polymers. However, with an increase in polymer concentration, phase separation is driven by the direct particle aggregation arising from the depletion of polymers. Because the particle phase has lower concentration of polymers, the number of bridges are also seen to become reduced.

The results in Figures 3a−d display the effect of the charge on the particles on the overall phase behavior. At higher Q_{net}, there is seen to be an increase in the region occupied by complex coacervates involving polymer-bridged phase (indicated by the red points on the phase diagram). Such phase behavioral features are also seen to be supported by the bridging fraction, B_r, which is seen to increase with an increase in particle charge (cf. Figure 3e). Similar trends were observed in the morphological phase diagrams presented in Pandav et al.[18] (cf. Figures 13a−d in the article). With an increase in the net charge of the particles, the volume fraction of particles in the particle-rich phase is seen to decrease for both the coacervate and the agglomerate phases. Such results can be rationalized by arguing that with an increase in the net charge of the particles the electrostatic repulsion between particles increases, leading to a decrease in particle volume fractions in the particle-rich phase. The corresponding increase in the bridging fractions can be rationalized by the fact that with an increase in the Q_{net} the adsorption of oppositely charged polyelectrolytes is enhanced, leading to the increased propensity to form polymer bridges.

To summarize, at low concentration of polymers, phase separation resembling complex coacervation is seen to result. The region (in polymer concentration plane) in which such a phase separation manifests increases with an increase in the net charge of the particles. With an increase in polymer concentration, the short-range attraction due to polymer depletion becomes dominant, leading to phase separation into particle-rich and polymer-rich phases.

4.2. Influence of Charge Heterogeneity of Proteins. In this section, we present results probing the effect of protein charge heterogeneity on the phase behavior of protein−PE mixtures. Such studies were motivated by observations which have demonstrated that proteins often exhibit heterogeneous charge patches arising from the distribution of different chemical groups on the solvent exposed surface.[42−46] In addition, a number of recent experiments have hinted at the possible nontrivial influence of such protein charge heterogeneity on protein−polyelectrolyte complexation characteristics.[43,47−52] Such experiments have commonly been interpreted as a consequence of the complexation between local patches on the protein of opposite charge to that of the polyelectrolyte.

Motivated by the above issues, in our previous study,[23] we probed the influence of charge heterogeneity on the structure of protein−polyelectrolyte complexes. For positive polyampholyte cases, the particles were seen to form either polymer-bridged or direct particle aggregates. Increasing the charge on the positive patches and/or the particle volume fractions led to an increased tendency to form particle aggregates. Increasing the number of patches (for fixed Q_p and Q_n) promoted the formation of polymer-bridged structures.

In this study, we sought to go beyond the above framework and use direct simulations of the phase behavior to probe the role of particle charge heterogeneity on the characteristics discussed in the preceding section. Toward this objective, we first maintained the net particle charge at $Q_{net} = 60$ and the polymer net charge at $Q_{pol} = 60$ and compare the results among three models for particle charge heterogeneity: PI0, PI1, and PI2. Subsequently, the net charge of the particle ($Q_{net} = Q_p - Q_n = 60$) was maintained fixed, while the ratio of Q_p to Q_n was varied.

Figure 4a presents results for the coacervate region of the phase diagram for PI0, PI1, and PI2 particles. Relative to the PI0 particles, the formation of coacervate phases is seen to extend to a higher concentration of polymers for both PI1 and PI2 particles. Such an observation is also supported by a higher bridging fraction (shown in Figure 4b,c) for PI1 and PI2 particles relative to PI0 particles at all polymer concentrations.

The above trends in phase behaviors are qualitatively consistent with the results presented in our previous publication.[23] Explicitly using the RDFs and morphological phase diagrams, it was shown that proteins with charge heterogeneity (i.e., PI1 and PI2 particles) exhibited a higher propensity to form PE bridges when compared to homogeneously charged particles. Similar results were reported by Kim et al. in which their patchiness parameter was found to correlate well with the phase behavior of the protein−polymer mixtures, and the formation of soluble aggregates was promoted by increasing the patchiness.[53] However, for the infinite dilution case studied in our earlier work,[23] we observed a decrease in the polymer bridging for particles exhibiting a larger degree of charge heterogeneity (such as PI2). Interestingly, such trends are not observed very distinctly in the phase behavioral characteristics shown in Figure 4a.

The higher propensity for complexation in PI1 and PI2 particles relative to PI0 particles can be understood to arise due to the presence of both negative and positive patches in PI1 and PI2 particles. The presence of oppositely charged patches on the particles gives rise to an additional interparticle attraction relative to the existence of only electrostatic repulsion among PI0 particles. This increased interparticle attraction causes the particles to be at closer proximity than PI0 particles, causing an increase in the bridge formation (and complexation) by oppositely charged polymers. At higher concentration of polymers, the bridging fractions of PI1 and PI2 particles are seen to be higher than PI0 particles; however, the influence of charge heterogeneity is seen to be more mitigated for such conditions due to the increased electrostatic screening arising from the higher concentrations of polymer.

To probe further the effects of particle charge heterogeneity and the electrostatic interactions between the oppositely charged patches, we adopted a framework in which the net charge of the particle ($Q_{net} = Q_p - Q_n = 60$) was maintained fixed, while the ratio of Q_p to Q_n was varied.

Figures 5a,b displays the results for the phase boundaries and the bridging fractions for the case in which the net charge of the particle ($Q_{net} = Q_p - Q_n = 60$) was maintained fixed, while the ratio of Q_p to Q_n was varied. The results show that the volume fraction of particles in the coacervate phases increases with an increase in the value of Q_p. In line with the results for phase behaviors, the fraction of polymers forming a bridge between two particles are seen to become enhanced with an increase in Q_p (cf. Figure 5b).

To rationalize the above observations, we recall that in our model framework increasing the value Q_p leads to an increase in Q_n to keep the net charge constant. As we discussed in the context of the results in Figure 4, the particle−particle electrostatic interaction for the heterogeneously charged particles is influenced by the product $Q_p \times Q_n$. Therefore,

https://dx.doi.org/10.1021/acs.jpcb.0c08317
J. Phys. Chem. B 2020, 124, 10943−10951

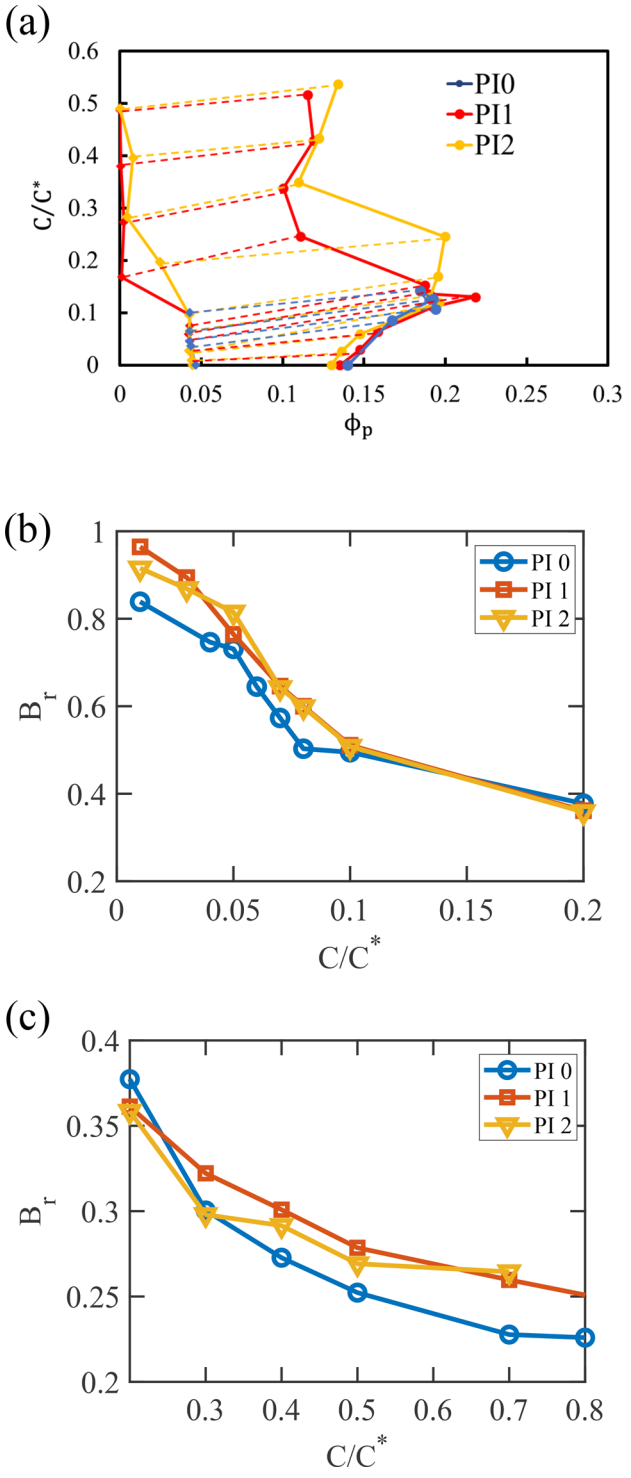

Figure 4. (a) Influence of charge heterogeneity on the phase behavior of protein−PE mixtures. Bridging fractions as a function of polymer bulk concentration for particles with a varying number of patches at (b) low polymer concentrations and (c) high polymer concentrations. For all the results, the net charge of the particles are constant at Q_{net} = 60 and Q_{pol} = 60. For PI1 and PI2 particles, Q_p = 80 and Q_n = 20.

with an increase in Q_p, the interparticle attraction increases, leading to a higher volume fraction of particles in the particle phase.

In summary, the results presented in this section demonstrate that relative to the homogeneously charged particles, patchy particles with both positive and negative

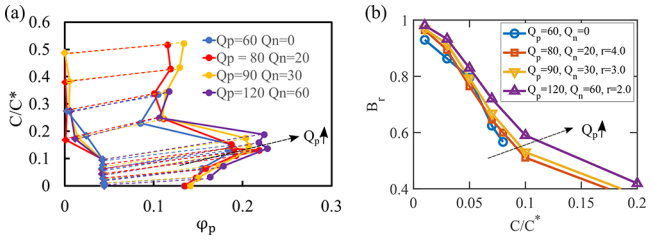

Figure 5. (a) Phase diagrams for PI1 particles with varying values of Q_p. (b) Bridging fractions as a function of polymer bulk concentration for PI1 particles with varying values of Q_p. For all the results, the net charge of the particles are constant at Q_{net} = 60 and Q_{pol} = 60.

patches (PI1, PI2) are more prone to form PE-bridged coacervates. Such a behavior was argued to arise from the additional attractive electrostatic interactions between the oppositely charged patches. With an increase in Q_p (while keeping Q_{net} fixed), the particle-rich portion of the phase boundary moved toward a higher volume fraction of the particles. Interestingly, within the small range of patchy particles investigated in this work, the number of patches on the particle did not exert a significant effect on the phase diagrams and the polymer bridging fractions.

5. CONCLUSIONS

We explored a single chain in the mean-field-based framework to probe the phase diagram of protein and PE mixtures. We used this framework to study the phase behavior of mixtures of PEs, and homogeneous and heterogeneously charged particles and studied the effect of net charge, charge distribution, and polymer concentration. In this study, we have used a model in which the charge of the proteins and the PEs are assumed to be completely dissociated and constant. Through the compositions of the coexisting phases and a characterization of the bridging fractions we showed that such mixtures form PE-bridged coacervate phases at high net particle charge and low PE concentration. However, at high PE concentration, the polymer depletion interactions became more important and led to segregative phase separation. Relative to homogeneously charged systems, particles exhibiting charge heterogeneity exhibited greater propensity to form PE-bridged coacervate phases.

The results of this present study serve to confirm and validate the conclusions presented in our earlier articles.[18,22,23] More broadly, our work also demonstrates the potential of the simulation framework to probe more complex phenomena in such systems such as the influence of partial dissociability of particle and polymer charges[24] and particle polymer size asymmetries. We plan to undertake such studies in our future work.

■ ASSOCIATED CONTENT

Supporting Information

The Supporting Information is available free of charge at https://pubs.acs.org/doi/10.1021/acs.jpcb.0c08317.

Figures S1−S3 (PDF)

■ AUTHOR INFORMATION

Corresponding Author

Venkat Ganesan − *Department of Chemical Engineering, University of Texas at Austin, Austin, Texas 78712, United*

https://dx.doi.org/10.1021/acs.jpcb.0c08317
J. Phys. Chem. B 2020, 124, 10943−10951

States; orcid.org/0000-0003-3899-5843;
Email: venkat@che.utexas.edu

Author

Rituparna Samanta − *Department of Chemical Engineering, University of Texas at Austin, Austin, Texas 78712, United States*

Complete contact information is available at: https://pubs.acs.org/10.1021/acs.jpcb.0c08317

Notes

The authors declare no competing financial interest.

■ ACKNOWLEDGMENTS

The National Science Foundation (Grant DMR-1721512) and the Robert A. Welch Foundation (Grant F-1599) both supported this work. The results in this paper were generated by using high performance computing resources provided by The University of Texas at Austin Texas Advanced Computing Center.

■ REFERENCES

(1) Euston, S. In *Food Microstructures*; Morris, V., Groves, K., Eds.; Woodhead Publishing Series in Food Science, Technology and Nutrition; Woodhead Publishing: 2013; pp 336−385.
(2) Grinberg, V.; Tolstoguzov, V. Thermodynamic incompatibility of proteins and polysaccharides in solutions. *Food Hydrocolloids* **1997**, *11*, 145−158.
(3) Khan, B. M.; Cheong, K.-L.; Liu, Y. ATPS: "Aqueous two-phase system" as the "answer to protein separation" for protein-processing food industry. *Crit. Rev. Food Sci. Nutr.* **2019**, *59*, 3165−3178.
(4) Schmitt, C.; Turgeon, S. L. Protein/polysaccharide complexes and coacervates in food systems. *Adv. Colloid Interface Sci.* **2011**, *167*, 63−70.
(5) Mohan, A.; Rajendran, S. R. C. K.; He, Q. S.; Bazinet, L.; Udenigwe, C. C. Encapsulation of food protein hydrolysates and peptides: a review. *RSC Adv.* **2015**, *5*, 79270−79278.
(6) Sureka, H. V.; Obermeyer, A. C.; Flores, R. J.; Olsen, B. D. Catalytic Biosensors from Complex Coacervate Core Micelle (C3M) Thin Films. *ACS Appl. Mater. Interfaces* **2019**, *11*, 32354−32365.
(7) Xu, Y.; Mazzawi, M.; Chen, K.; Sun, L.; Dubin, P. L. Protein Purification by Polyelectrolyte Coacervation: Influence of Protein Charge Anisotropy on Selectivity. *Biomacromolecules* **2011**, *12*, 1512−1522.
(8) Xu, Y.; Liu, M.; Faisal, M.; Si, Y.; Guo, Y. Selective protein complexation and coacervation by polyelectrolytes. *Adv. Colloid Interface Sci.* **2017**, *239*, 158−167.
(9) Armstrong, J. P. K.; Olof, S. N.; Jakimowicz, M. D.; Hollander, A. P.; Mann, S.; Davis, S. A.; Miles, M. J.; Patil, A. J.; Perriman, A. W. Cell paintballing using optically targeted coacervate microdroplets. *Chem. Sci.* **2015**, *6*, 6106−6111.
(10) de Kruif, C. G.; Weinbreck, F.; de Vries, R. Complex coacervation of proteins and anionic polysaccharides. *Curr. Opin. Colloid Interface Sci.* **2004**, *9*, 340−349.
(11) Kayitmazer, A. B. Thermodynamics of complex coacervation. *Adv. Colloid Interface Sci.* **2017**, *239*, 169−177.
(12) Turgeon, S.; Beaulieu, M.; Schmitt, C.; Sanchez, C. Protein-polysaccharide interactions: phase-ordering kinetics, thermodynamic and structural aspects. *Curr. Opin. Colloid Interface Sci.* **2003**, *8*, 401−414.
(13) Groenewold, J.; Kegel, W. K. Anomalously Large Equilibrium Clusters of Colloids. *J. Phys. Chem. B* **2001**, *105*, 11702−11709.
(14) Jones, O.; Decker, E. A.; McClements, D. J. Thermal analysis of β − lactoglobulin complexes with pectins or carrageenan for production of stable biopolymer particles. *Food Hydrocolloids* **2010**, *24*, 239−248.
(15) Russel, W. B.; Saville, D. A.; Schowalter, W. R. *Colloidal Dispersions*; Cambridge University Press: 1989; Vol. *54*, pp 201−202.
(16) Carlsson, F.; Linse, P.; Malmsten, M. Monte Carlo Simulations of Polyelectrolyte−Protein Complexation. *J. Phys. Chem. B* **2001**, *105*, 9040−9049.
(17) Skepö, M.; Linse, P. Dissolution of a polyelectrolyte-macroion complex by addition of salt. *Phys. Rev. E: Stat. Phys., Plasmas, Fluids, Relat. Interdiscip. Top.* **2002**, *66*, 051807.
(18) Pandav, G.; Pryamitsyn, V.; Errington, J.; Ganesan, V. Multibody Interactions, Phase Behavior, and Clustering in Nanoparticle-Polyelectrolyte Mixtures. *J. Phys. Chem. B* **2015**, *119*, 14536−14550.
(19) Kizilay, E.; Kayitmazer, A. B.; Dubin, P. L. Complexation and coacervation of polyelectrolytes with oppositely charged colloids. *Adv. Colloid Interface Sci.* **2011**, *167*, 24−37.
(20) Zhang, L.; Lu, D.; Liu, Z. How native proteins aggregate in solution: A dynamic Monte Carlo simulation. *Biophys. Chem.* **2008**, *133*, 71−80.
(21) Bolhuis, P. G.; Louis, A. A. How To Derive and Parameterize Effective Potentials in Colloid−Polymer Mixtures. *Macromolecules* **2002**, *35*, 1860−1869.
(22) Pandav, G.; Pryamitsyn, V.; Ganesan, V. Interactions and Aggregation of Charged Nanoparticles in Uncharged Polymer Solutions. *Langmuir* **2015**, *31*, 12328−12338.
(23) Samanta, R.; Ganesan, V. Influence of protein charge patches on the structure of protein − polyelectrolyte complexes. *Soft Matter* **2018**, *14*, 9475−9488.
(24) Samanta, R.; Halabe, A.; Ganesan, V. Influence of Charge Regulation and Charge Heterogeneity on Complexation between Polyelectrolytes and Proteins. *J. Phys. Chem. B* **2020**, *124*, 4421−4435.
(25) Gubbins, K. E. The Role of Computer Simulation in Studying Fluid Phase Equilibria. *Mol. Simul.* **1989**, *2*, 223−252.
(26) Panagiotopoulos, A. Z. Direct Determination of Fluid Phase Equilibria by Simulation in the Gibbs Ensemble: A Review. *Mol. Simul.* **1992**, *9*, 1−23.
(27) Gartner, T. E.; Jayaraman, A. Modeling and Simulations of Polymers: A Roadmap. *Macromolecules* **2019**, *52*, 755−786.
(28) Panagiotopoulos, A. Z. Gibbs Ensemble Techniques. In *Observation, Prediction and Simulation of Phase Transitions in Complex Fluids*; Springer: 1995.
(29) Escobedo, F. A.; de Pablo, J. J. Expanded grand canonical and Gibbs ensemble Monte Carlo simulation of polymers. *J. Chem. Phys.* **1996**, *105*, 4391−4394.
(30) Koski, J. P.; Krook, N. M.; Ford, J.; Yahata, Y.; Ohno, K.; Murray, C. B.; Frischknecht, A. L.; Composto, R. J.; Riggleman, R. A. Phase Behavior of Grafted Polymer Nanocomposites from Field-Based Simulations. *Macromolecules* **2019**, *52*, 5110−5121.
(31) Koski, J.; Chao, H.; Riggleman, R. A. Field theoretic simulations of polymer nanocomposites. *J. Chem. Phys.* **2013**, *139*, 244911.
(32) Chao, H.; Koski, J.; Riggleman, R. A. Solvent vapor annealing in block copolymer nanocomposite films: a dynamic mean field approach. *Soft Matter* **2017**, *13*, 239−249.
(33) Doi, M.; Edwards, S. *The Theory of Polymer Dynamics*; Clarendon Press: 1988.
(34) Fredrickson, G. H. *The Equillibrium Theory of Inhomogenous Polymers*; Oxford Science: 2006.
(35) Daoulas, K. C.; Müller, M. Single chain in mean field simulations: Quasi-instantaneous field approximation and quantitative comparison with Monte Carlo simulations. *J. Chem. Phys.* **2006**, *125*, 184904.
(36) Detcheverry, F. A.; Kang, H.; Daoulas, K. C.; Müller, M.; Nealey, P. F.; de Pablo, J. J. Monte Carlo Simulations of a Coarse Grain Model for Block Copolymers and Nanocomposites. *Macromolecules* **2008**, *41*, 4989−5001.
(37) Müller, M.; Daoulas, K. C. Calculating the free energy of self-assembled structures by thermodynamic integration. *J. Chem. Phys.* **2008**, *128*, 024903.

(38) Metropolis, N.; Rosenbluth, A. W.; Rosenbluth, M. N.; Teller, A. H.; Teller, E. Equation of State Calculations by Fast Computing Machines. *J. Chem. Phys.* **1953**, *21*, 1087−1092.
(39) Pryamitsyn, V.; Ganesan, V. Pair interactions in polyelectrolyte-nanoparticle systems: Influence of dielectric inhomogeneities and the partial dissociation of polymers and nanoparticles. *J. Chem. Phys.* **2015**, *143*, 164904.
(40) Pryamitsyn, V.; Ganesan, V. Interplay between Depletion and Electrostatic Interactions in PolyelectrolyteNanoparticle Systems. *Macromolecules* **2014**, *47*, 6095−6112.
(41) Samanta, R.; Ganesan, V. Influence of dielectric inhomogeneities on the structure of charged nanoparticles in neutral polymer solutions. *Soft Matter* **2018**, *14*, 3748−3759.
(42) Kayitmazer, A. B.; Quinn, B.; Kimura, K.; Ryan, G. L.; Tate, A. J.; Pink, D. A.; Dubin, P. L. Protein Specificity of Charged Sequences in Polyanions and Heparins. *Biomacromolecules* **2010**, *11*, 3325−3331.
(43) Dubin, P. L.; Gao, J.; Mattison, K. Protein Purification by Selective Phase Separation with Polyelectrolytes. *Sep. Purif. Methods* **1994**, *23*, 1−16.
(44) Laos, K.; Brownsey, G.; Ring, S. Interactions between furcellaran and the globular proteins bovine serum albumin and-lactoglobulin. *Carbohydr. Polym.* **2007**, *67*, 116−123.
(45) da Silva, F. L. B.; Jonsson, B. Polyelectrolyte-protein complexation driven by charge regulation. *Soft Matter* **2009**, *5*, 2862−2868.
(46) Li, Y.; Zhao, Q.; Huang, Q. Understanding complex coacervation in serum albumin and pectin mixtures using a combination of the Boltzmann equation and Monte Carlo simulation. *Carbohydr. Polym.* **2014**, *101*, 544−553.
(47) Harnsilawat, T.; Pongsawatmanit, R.; McClements, D. J. Influence of pH and Ionic Strength on Formation and Stability of Emulsions Containing Oil Droplets Coated by-LactoglobulinAlginate Interfaces. *Biomacromolecules* **2006**, *7*, 2052−2058.
(48) Mattison, K. W.; Brittain, I. J.; Dubin, P. L. Protein"Polyelectrolyte Phase Boundaries. *Biotechnol. Prog.* **1995**, *11*, 632−637.
(49) Tsang, Y.; Thompson, T. E. The Use of Combined Schlieren and Absorption Optics in an Electrophoretic Study of the Reversibly Interacting System Dextran Sulfate"Carboxyhemoglobin1,2. *J. Phys. Chem.* **1965**, *69*, 4242−4249.
(50) Hofstee, B. Solubility and comparison of protein-deoxyribonucleic acid complexes. *Biochim. Biophys. Acta, Spec. Sect. Nucleic Acids Relat. Subj.* **1964**, *91*, 340−343.
(51) Lesins, V.; Ruckenstein, E. Patch controlled attractive electrostatic interactions between similarly charged proteins and adsorbents. *Colloid Polym. Sci.* **1988**, *266*, 1187−1190.
(52) Kopaciewicz, W.; Rounds, M.; Fausnaugh, J.; Regnier, F. Retention model for high-performance ion-exchange chromatography. *Journal of Chromatography A* **1983**, *266*, 3−21.
(53) Kim, S.; Sureka, H. V.; Kayitmazer, A. B.; Wang, G.; Swan, J. W.; Olsen, B. D. Effect of protein surface charge distribution on protein − polyelectrolyte complexation. *Biomacromolecules* **2020**, *21*, 3026−3037.

https://dx.doi.org/10.1021/acs.jpcb.0c08317
J. Phys. Chem. B 2020, 124, 10943−10951